Boron nitride nanotubes-based nanofluids with enhanced thermal properties for use as heat transfer fluids in solar thermal applications

Roberto Gomez-Villarejo, Patrice Estellé, Javier Navas

Boron nitride nanotubes-based nanofluids with enhanced thermal properties for use as heat transfer fluids in solar thermal applications

Roberto Gómez-Villarejo,[1] Patrice Estellé,[2] Javier Navas,[1,*]

[1] Departamento de Química Física, Facultad de Ciencias, Universidad de Cádiz, E-11510 Puerto Real (Cádiz), Spain;

[2] Univ Rennes, LGCGM, EA3913, F-35000 Rennes, France

Corresponding Author:

*Javier Navas (javier.navas@uca.es)

Abstract

Nanofluids are considered as promising alternative in heat exchange processes to the classical fluids, which usually present poor thermal properties. One interesting application for nanofluids is as heat transfer fluid in solar thermal applications plants. Boron nitride nanotubes present interesting thermophysical properties for use in nanofluids. Therefore, nanofluids based on boron nitride nanotubes were prepared by a two-step method, dispersing this nanomaterial in a heat transfer fluid typically used. Stability, rheological and thermal properties of the nanofluids were analysed. To check the stability, ultraviolet-visible spectroscopy and particle size and ζ-potential measurements were performed for a month, obtaining that the nanofluids were stable. Furthermore, surface tension was measured and no significant differences were observed with regard to the base fluid. In a variable range of temperature, nanofluids show Newtonian behaviour with a slight increase in viscosity. Besides, the boron nitride nanotubes caused an increase in thermal conductivity of up to 33% with regard to the base fluid. The use of these nanofluids also led to an improvement in the heat transfer coefficient under turbulent flow conditions of up to 18%. Finally, the analysis of the outlet temperature in solar thermal applications shows that these nanofluids are a promising alternative in this application.

Keywords: Concentrating Solar Power; Nanofluids; Boron nitride nanotubes; Thermal properties; Rheological properties.

1. Introduction

The concept “nanofluids” was proposed by Choi [1] in 1995 and they are defined as dispersion of nanometre size materials in a liquid. Over the last decade, a wide range of combinations of nanomaterials and fluids has resulted in nanofluids receiving a great deal of attention as a promising option for enhancing heat transfer and thermal properties with regard to conventional fluids such as water, ethylene glycol and engine oil. For example, using water as a base fluid, Teng et al. reported improvements for water/alumina nanofluids [2] or Gao et al. reported enhanced heat transfer properties for graphene nanoplatelet water-based nanofluid [3]. Also, using ethylene glycol as the base fluid, improvements in some thermal properties have been reported for nanofluids based on SiC [4], ZnO [5], SiO_2 [6],… Moreover, using oils, some nanofluids have been studied, for example the analysis of the layering and clustering phenomena in CuO-based nanofluids [7], the study of thermal and rheological properties of graphite-based nanofluids [8], or the analysis of the thermal properties and electrical insulation of h-BN based nanofluids in a dielectric oil [9]. A practical application for these nanofluids could possibly be found in the solar thermal industry, as in the emerging field of Concentrating Solar Power (CSP) [10, 11]. This new technology concentrates solar radiation in a receptor where solar energy is transformed into thermal energy, reaching high temperatures [12]. Receptors such as the tower power system, linear Fresnel, parabolic dish or parabolic trough collectors contain a heat transfer fluid, generally molten salt or thermal oil [13], which recirculates and is used to evaporate water for electricity generation.

Much of the research into the heat transfer enhancement of nanofluids has focused on metallic nanoparticles, for example Cu in synthetic oil [14], Cu/diethylene based nanofluids [15], or the comparison of the effect of Cu and Ni nanoparticles in thermal properties of nanofluids [16], and also on metallic oxide nanoparticles, such as the

analysis of the drastic enhancement of the thermal conductivity in NiO-based nanofluids for solar thermal applications [17], the study of alumina-based nanofluid in synthetic oil [18], and also using TiO_2 nanoparticles [19]. Recently, 2D nanomaterials [20] have appeared as an attractive alternative due to the high surface area they have available for heat transfer. Moreover, other current studies reporting interesting results have led to the development of 1D nanomaterials such as carbon nanotubes, which show good values of intrinsic thermal conductivity [21], and also have been used in water-based nanofluids with interesting results [22].

Belonging to the new field of 1D nanomaterials, boron nitride materials possess very similar structures to those showed by carbon materials, with analogous morphologies, similar mechanical properties and remarkable chemical inertness [23]. One of the first efforts to achieve boron nitride materials was carried out in 1981 by Ishii [24], who obtained whisker-like material on boron nitride and the perfect tubular boron nitride structure was synthesized in 1995 through an arc-discharge technique [25]. Many techniques were adapted to synthesize these materials, such as laser ablation [26] or chemical vapour deposition [27]. BN nanostructures, shaped like flakes, tubes or ribbons [28], are relatively new materials that have had repercussion on areas such as hydrogen storage [29], electronic structures [30] and, in particular, in the field of heat transfer [31]. The use of BN in production of nanofluids and the evaluation of their properties is a new and recent field of investigation as evidenced in the following short literature review on this topic. Li et al [32] prepared nanofluids based on boron nitride with different sized nanoparticles and ethylene glycol as the base fluid and demonstrated that nanofluids with larger nanoparticles had higher thermal conductivity than smaller ones. Zhi et al [23] worked with BN nanotubes (BNNTs) and BN nanospheres (BNNSs) and water as the base fluid, and they achieved 2.6 times and 1.6 times enhancement of thermal

conductivity compared to the base fluid for a 6 vol % fraction of BNNTs and BNNSs nanofluids, respectively. Taha-Tijerina et al [33] demonstrated high thermal conductivity in nanofluids with hexagonal boron nitride in mineral oil. İlhan et al [34] reported an enhancement of thermal conductivity for hexagonal BN nanofluids of up to 26%, 22% and 16% at volume concentrations of 3% for water, water/ethylene glycol mixture and ethylene glycol based nanofluids, respectively. Lastly, Michael et al. [35] investigated near spherical BN nanoparticles in the concentration range 0.5-3 in vol.% dispersed in ethylene glycol and a mixture of water/ethylene glycol. Thermal conductivity enhancement of these nanofluids is higher than 12% at 3 vol.% without change with temperature increase. However, such an enhancement is accompanied by a change in Newtonian behaviour of base fluid to shear-thinning with an increase in viscosity up to 40%. More recently, Gomez-Villarejo et al. [36] experimentally studied water-based nanofluids containing BN nanotubes with low volume fraction ranging from 0.08 to 0.25%. A maximum enhancement of 8% and 10% in isobaric heat capacity and thermal conductivity was respectively achieved at 70°C. Interestingly, such results were obtained with no significant change nor enhancement in rheological properties.

As continuation of this previous work for high temperature application, the current study reports the experimental investigation of the temporal stability, thermophysical and rheological properties, as well as the application in CSP plants of nanofluids based on BNNTs and a synthetic oil commonly used in this kind of plants. First, stability and all thermophysical properties are determined with regard to the amount of nanomaterial added and for wide range of temperature until 363K. Then, the possible application in CSP plants is evaluated by means of the estimation of heat transfer coefficient and the outlet temperature. The production and characterization of stable commercial thermal oil nanofluids using BNNTs is here done for the first time, and a significant improvement in

heat transfer processes is here originally reported leading to promising application in CSP.

2. Material and methods

2.1. Nanofluids preparation

The nanofluids were formulated by a two-step method [37] whereby the first process is the synthesis of nanomaterial and the second involves the dispersion of the nanomaterial into a base fluid. The base fluid was prepared by mixing the typical heat transfer fluid (HTF) used in CSP plants with an adequate amount of Triton X-100 that acts as surfactant. This HTF was Dowtherm A, the eutectic mixture of biphenyl ($C_{12}H_{10}$, 26.5%) and diphenyl oxide ($C_{12}H_{10}O$, 73.5%), supplied by The Dow Chemical Company©. Triton X-100 ($C_{14}H_{22}O(C_2H_4O)_n$, average molecular weight of 625, density: 1.07 g/cm^3, purchased by Panreac©,) is a non-ionic compound that has a hydrophilic polyethylene oxide chain and an aromatic hydrocarbon lipophilic or hydrophobic group which was used as a stabilizing agent to improve the stability of the nanomaterial in the base fluid, a common procedure with nanofluids [38]. The nanomaterial used was boron nitride nanotubes (BNNTs, purchased by Sigma-Aldrich©) with a BNNTs content over 50% and elemental boron free lower than 25%, and a surface area (BET) above 100 m^2/g. BNNTs were produced from inductively coupled plasma synthesis in the absence of metal catalysis according to the manufacturer's specification. While the manufacturer indicates an average nanotube diameter of about 5±2 nm, SEM characterization described earlier [36] and reported in Figure 1 shows the directionality of this nanomaterial, which creates an entanglement of nanotubes that have a diameter of around 20-30 nm. In addition, some impurities with a spherical morphology are also observed. Also, the density of BNNTs was previously evaluated from gas pycnometry to 1396.5 kg m^{-3} [36].

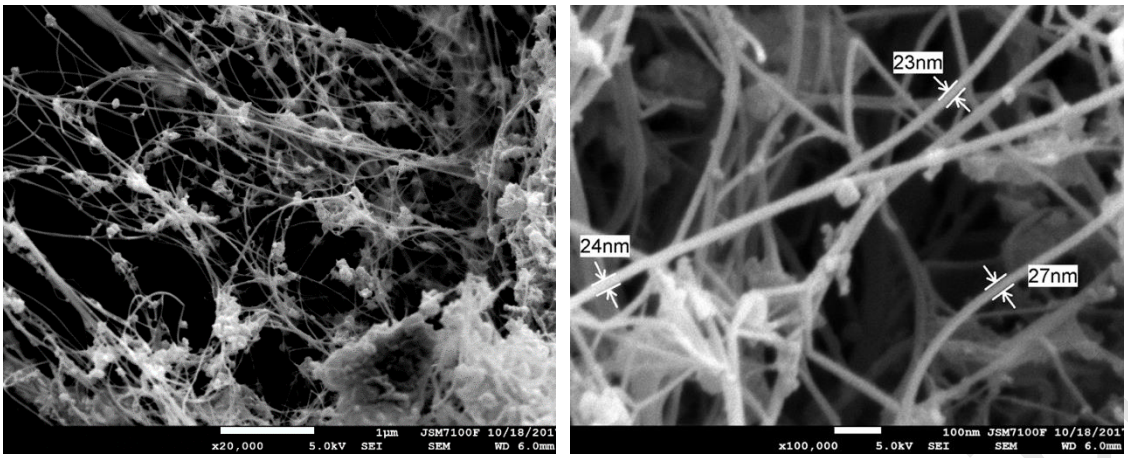

Figure 1. SEM images obtained for BNNTs used for preparing nanofluids.

To prepare the base fluid, an initial solution of base fluid with 0.35 vol.% of Triton X-100 was prepared and magnetically stirred for thirty minutes. Three nanofluids with different BNNT mass concentrations, $1 \cdot 10^{-3}$, $3 \cdot 10^{-3}$ and $5 \cdot 10^{-3}$ wt.% respectively were obtained from the dilution of the initial solution. A sonication method was used for the optimal dispersion of the nanomaterial in the base fluid. A frequency of 80 kHz was applied for 4 hours using an Elmasonic P by Elma®, the temperature being maintained below 303K in a thermal bath. A base fluid sample without nanomaterial was also prepared for comparison purposes.

2.2. Nanofluids characterization and performance

Several properties were measured to determine the stability of the nanofluids and the possible enhancement of their thermal properties with regard to the base fluid.

The stability of the nanofluids was tested by dynamic light scattering (DLS) measurements to obtain an accurate representation of nanoparticle size distribution. Another quantitative approach for determining the stability of the nanofluids was through ζ-potential measurements, to understand the interactions between the nanomaterial in suspension and therefore the agglomeration process. Both measurements were carried out

using a Zetasizer Nano ZS system supplied by Malvern Instruments© (Malvern, United Kingdom). In parallel, a follow-up to study the sedimentation processes was carried out by means of UV-Vis spectroscopy, using a system composed of a DH-2000-BAL halogen lamp as the light source and a USB200+ spectrometer, both devices supplied by Ocean Optics© (Ocean Optics, United Kingdom). The UV-vis spectra, particle size and ζ-potential measurements were recorded several times each day for 30 days.

Several thermophysical properties were also analysed in this work to determine the efficiency of the nanofluids because they are involved in the heat transfer coefficient (*h*), as evidenced in [39]. Therefore, surface tension, density, viscosity, isobaric specific heat and thermal conductivity were characterized, from the experimental procedures described in the following, in order to evaluate the performance of the nanofluids.

Furthermore, surface tension (ST) at the interface between air and both the base fluid and nanofluids was measured employing the pendant drop technique with a KRÜSS GmBH DSA-30 Drop Shape Analyzer (Hamburg, Germany). As in our previous work [36], drops are produced within a temperature chamber at controlled temperature in the 283-323K temperature range after ten 10 mins at the required temperature. A 15-gauge needle with an outer diameter of 1.835 mm was use to generate drops keeping under control the flow rate and volume, as reported in literature [40]. Surface tension values are registered from a drop produced at the end of the needle and its shape analysis from the Young-Laplace equation. The reported ST values were measured at least ten times and no significant deviation was found between replicates. A maximum relative deviation of 0.1% was obtained with pendant drop calibration gauges at 293 K.

The density of the nanofluids was estimated by a pycnometer immerse in a thermal bath to keep the room temperature and the measurements were performed in triplicate. Moreover, rheological measurements were performed in a wide temperature range of

283K to 363K with a Malvern Kinexus Pro stress-controlled rheometer (Malvern Instruments Ltd©, United Kingdom) working with a cone-and-plate geometry under steady-state conditions. The angle and diameter of the cone were 60 mm and 1º respectively. Measurements were taken imposing a logarithmic shear stress ramp which was selected to cover a shear rate range between 100 and 1000 s^{-1} for each sample. Temperature was established and controlled by a Peltier temperature control system with a precision of ±0.1K, and this system was linked to thermal clovers to ensure a constant temperature within the sample gap during measurements. The samples were left at the required temperature for five minutes before beginning the experiments. The number of points per decades was adjusted to avoid sample evaporation during measurement. Evaporation cannot be controlled at temperatures higher than 363K. A comprehensive description of this experimental procedure and uncertainty evaluation in viscosity lower than 4% were reported earlier [41]. Viscosity of Dowtherm A, the base fluid (Triton X-100 solution in Dowtherm A) and all nanofluids prepared was measured in several replicates to evaluate the influence of the surfactant and the nanoparticle content respectively.

Isobaric specific heat measurements were taken using a Temperature Modulated Differential Scanning Calorimeter (TMDSC), supplied by Netzsch© model DSC214 Polyma. The experiments were performed in aluminium crucibles and a standard procedure was established to perform the measurements, which can be summarized as follows: the temperature was equilibrated at 341K to remove contaminants or impurities and kept isothermal for 10 min; then the samples were equilibrated at 288K and then ramped to 373K at 1 K/min. A modulation was programmed around the studied temperatures with an amplitude of ± 1 K and a period of 120 s. Finally, the samples were

allowed to cool freely. Isobaric specific heat values were estimated based on the ratio method with a sapphire standard sample as a reference of known thermal properties.

Finally, thermal diffusivity, defined as the speed of heat propagation by conduction during changes of temperature, was analysed by the laser flash technique, using LFA467 HyperFlash equipment, supplied by Netzsch©. The thermal conductivity (k) is estimated by the relationship between thermal diffusivity (D), isobaric specific heat (C_P) and density (ρ), given by the equation [42].

$$k(T) = D(T) \cdot C_P(T) \cdot \rho(T) \tag{1}$$

On the other hand, taking into account the properties measured, the possible enhancement of the heat transfer process under turbulent and laminar flow conditions can be verified. Under turbulent flow conditions such as those found in CSP plants, the Dittus-Boelter equation was used as a *Figure of Merit* (*FoM*) [43]. This *FoM* gives the ratio between the heat transfer coefficient (h) of the nanofluids with regard to the base fluid, which depends on density, thermal conductivity, isobaric specific heat and dynamic viscosity (μ). Mathematically, it is defined as

$$FoM = \frac{h_{nf}}{h_{bf}} = \left(\frac{\rho_{nf}}{\rho_{bf}}\right)^{0.8} \left(\frac{k_{nf}}{k_{bf}}\right)^{0.6} \left(\frac{C_{p(nf)}}{C_{p(bf)}}\right)^{0.4} \left(\frac{\mu_{nf}}{\mu_{bf}}\right)^{-0.4} \tag{2}$$

where all variables have been defined previously and subscripts *nf* and *bf* is referred to nanofluid and base fluid, respectively. An improvement in the heat transfer efficiency is considered when $h_{nf} / h_{bf} > 1$. Such an expected improvement has to be evaluated with regards of possible enhancement of friction factor due to the presence of nanoparticles

that modify the thermophysical properties of base fluids. For turbulent flow and smooth pipe absorber generally encountered in CSP and parabolic collector, the friction factor can be evaluated from the following equation in the range Re = 3000–10^8 [44]:

$$f = 0.25\left[log\left(\frac{150.39}{Re^{0.98865}} - \frac{152.66}{Re}\right)\right]^{-2} \quad (3)$$

where *Re* is defined by the following equation $Re = \rho V_{av} D/\mu$ with ρ and μ the density and the dynamic viscosity of fluids respectively, V_{av} and D being the average fluid velocity in the inner pipe and the inner pipe diameter.

Also, according to the criterion of Prasher [45], under laminar flow conditions a nanofluid is considered to improve the efficiency when the dynamic viscosity increase (DVI) is less than four times the thermal conductivity enhancement (TCE), expressed mathematically as:

$$\frac{DVI}{TCE} = \frac{\left(\mu_{nf} - \mu_{bf}\right)/\mu_{bf}}{\left(k_{nf} - k_{bf}\right)/k_{bf}} \leq 4 \quad (4)$$

where all variables and subscripts have been previously defined. Both *FoMs* have been evaluated for the nanofluids prepared.

On the other hand, it is possible to analyse the effect of the use of nanofluids on the efficiency by means of the analyse of the useful energy production (Q_u), which is defined as[46, 47]

$$Q_u = \mathrm{h} \cdot \mathrm{A} \cdot \left(T_s - T_{fm}\right) \quad (5)$$

where A is the area of the inner receiver, T_s is the temperature of the receiver, and T_{fm} is the mean fluid temperature. In this sense, higher values of h lead to lower values of T_s and consequently to lower thermal losses, and therefore the collector thermal efficiency increases.

Finally, for its potential application in CSP plants, which work at high temperature, the nanofluid with the highest volume fraction of BNNTs was used in successive thermal cycles. The nanofluid was heated for 5 hours controlling the evaporation of the fluid at 573 K without stirring. Before and after of each cycle, measurements of extinction coefficient at λ=335 nm and particle size were performed to observe any variation in amount and size distribution of the nanomaterial in suspension. Also, the morphology of the nanomaterial has been checked out before and after of thermal cycles by means of transmission electron microscopy using a FEI© Talos F200s X Twin Microscope in Scanning Transmission Electron Microscopy (STEM) mode.

2.3. Thermal conductivity models

An analysis using several models to evaluate the thermal conductivity with regard to volume fraction may be of interest in order to understand the way in which the heat conduction into the nanofluids takes place. The thermal conductivity enhancement predicted by Maxwell´s model [48] of a homogenous suspension can be presented as:

$$\frac{k_{nf}}{k_{bf}} = \frac{k_p + 2k_{bf} + 2\left(k_p - k_{bf}\right)\phi}{k_p + 2k_{bf} - \left(k_p - k_{bf}\right)\phi} \tag{6}$$

where k_{nf} and k_{bf} correspond to thermal conductivity of the nanofluid and base fluid respectively, and k_p is the thermal conductivity of the BNNTs, which is 46 W m^{-1} $^oC^{-1}$

[31]. Also, ϕ is the volume fraction, which is calculated as $\phi = (\rho_{nf} - \rho_{bf})/(\rho_{nt} - \rho_{bf})$, where the subscript *nt* is related to BN nanotubes, and the rest of variables and subscripts have been defined previously. Hamilton and Crosser (H-C) [49] proposed a model for liquid-solid mixtures of non-spherical particles, considering the shape of the nanomaterial, which is not taken into account in the Maxwell model. The H-C model is defined as

$$\frac{k_{nf}}{k_{bf}} = \frac{k_p + (n-1)k_{bf} + (n-1)(k_p - k_{bf})\phi}{k_p + (n-1)k_{bf} - (k_p - k_{bf})\phi} \tag{7}$$

where *n* is the shape factor, usually defined as $n = 3/\psi$, ψ being the sphericity, which can be calculated from the dimensions of the nanomaterial. Nevertheless, an analysis of BNNTs reveals a lack of knowledge about their dimension in this case and consequently the use of the H-C model is not recommended. Many models have been reported for predicting thermal conductivity of nanofluids based on spherical nanoparticles, but there are few specific models for nanotubes. One example is the Xue model [50]:

$$\frac{k_{nf}}{k_{bf}} = \frac{1 - \phi + 2\phi \frac{k_p}{k_p - k_{bf}} ln \frac{k_p + k_{bf}}{2k_{bf}}}{1 - \phi + 2\phi \frac{k_{bf}}{k_p - k_{bf}} ln \frac{k_p + k_{bf}}{2k_{bf}}} \tag{8}$$

where all the variables have been previously defined. On the other hand, new models take into account contributions to other conduction mechanisms, such as the Brownian motion. Thus, assuming that this mechanism can be considered separately, the total effective thermal conductivity can be considered as the sum of the terms related to static conductivity and Brownian motion; that is, $k_{nf} = k_{static} + k_{brownian}$. Thus, to take into

account dynamic transport, Xuan et al. reported a model that includes the influence of viscosity, temperature and other properties of the base fluid and the nanoparticles, given by [51]:

$$k_{brownian,Xuan} = \frac{\rho_p \phi C_{P,bf}}{2} \sqrt{\frac{\kappa T}{3\pi \mu r_c}} \quad (9)$$

where ρ_p is the density of BNNTs (1396.6 kg m^{-3}), $C_{P,bf}$ is the isobaric specific heat of the base fluid, κ is the Boltzmann constant, μ the viscosity and r_c is the mean gyration radius of the cluster. This value is estimated from the DLS measurements shown above when the nanofluids are considered stable. An average of the two distributions found considering the proportion of each one was calculated. Therefore, in this work, combinations of the Maxwell and Xue model for static conduction and the Brownian contribution reported by Xuan have been considered.

3. Results and discussion

3.1. Nanofluid stability

To use a nanofluid as heat transfer fluid, one important issue is to obtain a stable and durable suspension. To consider a nanofluid as a stable system, the concentration of nanomaterial in suspension should be stable over time [52]. The stability of nanofluids is a decisive parameter to study before determining any possible enhancement of thermal properties [23]. Agglomeration and precipitation occur immediately after nanofluid preparation due to Van der Waals attraction force between different compounds, and these phenomena have a negative impact on thermal conductivity [53]. Li et al [32] showed a

tendency of boron nitride powder to create “cloud-like compact aggregations”. In turn, a widespread way to achieve good stability is by the use of surfactants [38, 54]. Moreover, sonication is required to assure the optimum dispersion of a nanomaterial into a base fluid [28, 32].

To verify the stability of the BNNT nanofluids, they were analysed using several techniques described in section 2.2. UV-Vis spectra were recorded in a range of 300-800 nm for all the nanofluids after their preparation to analyse agglomeration and sedimentation processes. The nanofluids showed a wide band centred at lower wavelengths due to the presence of nanomaterial in suspension, this type of band being typical for colloidal suspension systems. This phenomenon is known to mainly take place at lower wavelengths [55]. Therefore, the extinction signal of incident radiation measured at λ=335 nm was analysed for one month, and the variations in signal are shown in Figure 2. The extinction decreased in every nanofluid at first, but we can consider all the nanofluids as stable after the 15^{th} day, when the extinction values remained practically constant. Figure 2 also shows that the decrease in the extinction value is practically the same for the three nanofluids, which indicates that the range of variation of the concentration of nanomaterial in suspension is the same rate in all cases.

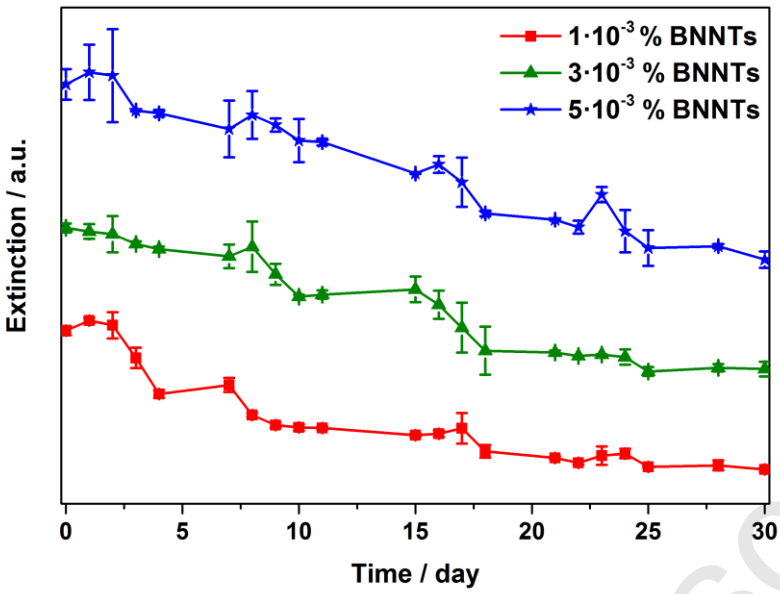

Figure 2. Extinction values registered at λ=335 nm for the nanofluids prepared.

The DLS technique was used to measure particle sizes to analyse the agglomeration process. This technique really measures the hydrodynamic radius, which is determined as the sum of the particle diameter and the Debye length. The Debye length is the thickness of the diffuse layer, a layer of species between the surface of the nanoparticle and the slipping plane that moves with the nanoparticle within the base fluid. For this reason, the value obtained using this technique always overestimates the size of the particles [56]. The particle size values for the nanofluids are shown in Figure 3a-c. Two different size distributions in each nanofluid are observed, one of them in values at about 200-300 nm, and the second one around 400-600 nm. Figure 3d shows the relative intensity of these peaks obtained in most cases. Zyla et al. [57] describe the existence of a characteristic bimodal size distribution in boron nitride nanoparticles based on ethylene glycol nanofluids, with values of 192 nm and 2969 nm. In this case, it would be reasonable to think that the presence of the two peaks is the result of an agglomeration phenomenon of

the nanotubes [32], which form structures with a regular size due to the presence of the surfactant, which prohibits further agglomeration.

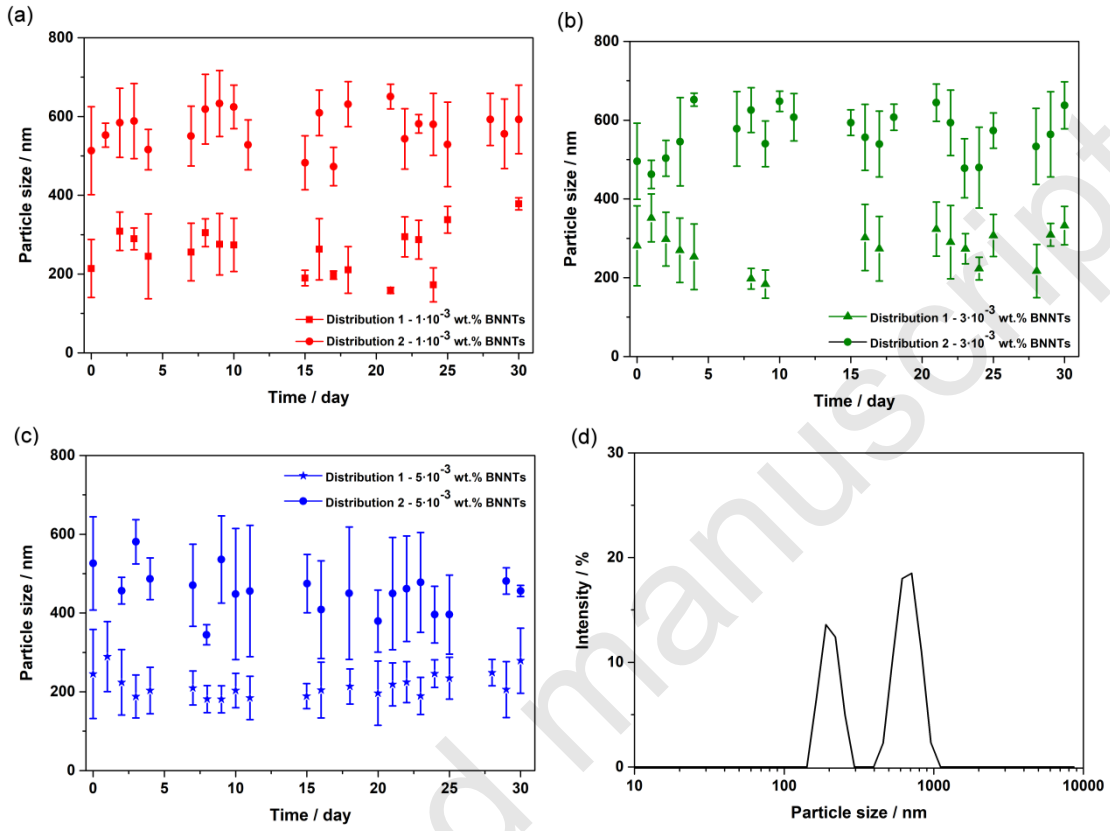

Figure 3. Particle size values obtained for the nanofluids prepared with 1·10-3 wt.% (a), 3·10-3 wt.% (b) and 5·10-3 wt.% (c) of BNNTs. (d) Typical bimodal size distribution obtained for the nanofluids prepared (in this case, this plot was obtained for the nanofluid with 3·10-3 wt.% of BNNTs).

Finally, Figure 4 shows the ζ-potential values obtained for the nanofluids. A nanofluid is considered stable when presents values of ζ-potential higher than 20-30 mV [58], in absolute values. After the first few days, all the values obtained were constant for each nanofluid, exhibiting a certain relationship between the concentration of BNNTs and zeta potential. Thereby, the nanofluid with $0.1 \cdot 10^{-3}$ wt. % presented a ζ-potential around -20

mV. The nanofluid with $0.3 \cdot 10^{-3}$ wt. % presented values of ζ-potential around -30 mV, and lastly, the nanofluids with the highest concentration of BNNTS, $0.5 \cdot 10^{-3}$ wt. %, presented a ζ-potential around -40 mV. These results are similar to those obtained by Taha-Tijerina et al. [9] for a 0.1 wt.% hexagonal boron nitride in mineral oil, and to those reported by Gomez-Villarejo et al. [36].

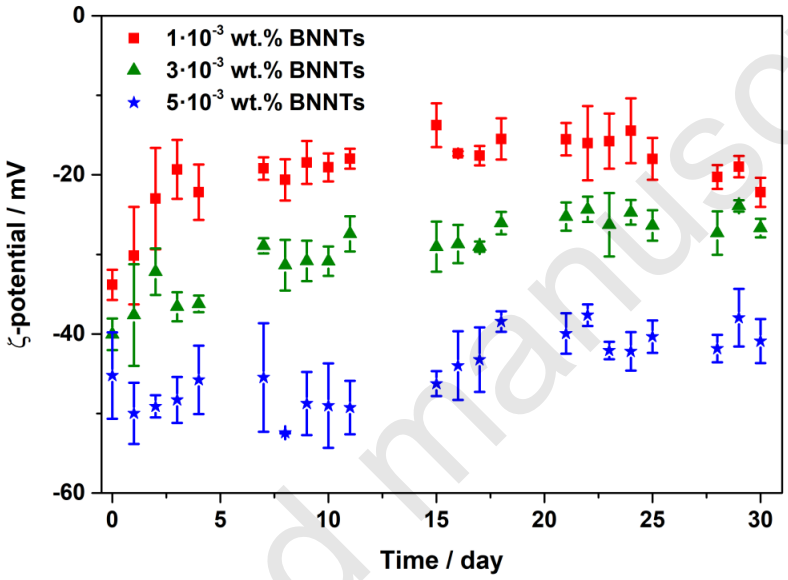

Figure 4. ζ-potential values obtained for the nanofluids prepared for a month.

These results show that in spite of the inherent phenomena of agglomeration suffered by this type of nanomaterial, a remarkable temporal stability can be observed and contrasted in the three nanofluids prepared.

3.2. Surface Tension measurements

Surface tension (ST) is a physical property which plays an important role in two-phase heat transfer flows, heat pipes and processes that involve boiling heat transfer and condensation [59]. First, a comparison of experimental surface tension values obtained

from Dowtherm A and values from the manufacturer are shown in Figure 5a to determine the precision of the procedure. As expected, the ST of Dowtherm A decreases with the increase in temperature, with an absolute average deviation percentage (AAD %) lower than 1.3%.

The influence of Triton-X 100 and BNNTs on ST is showed in Figure 5b. Also, the values obtained are shown in Table 1. The addition of surfactant causes an increase in ST values with regard to the Dowtherm A of around 1.2% at room temperature (close to experimental uncertainty) and 2.4% at 363 K. However, the presence of BNNTs did not produce significant changes in the ST values, indicating that surfactant is solely responsible for the changes observed in ST with regard to the Dowtherm A. Also, as expected, the ST of the base fluid and nanofluids decreased with temperature, following a similar trend to that obtained for Dowtherm A.

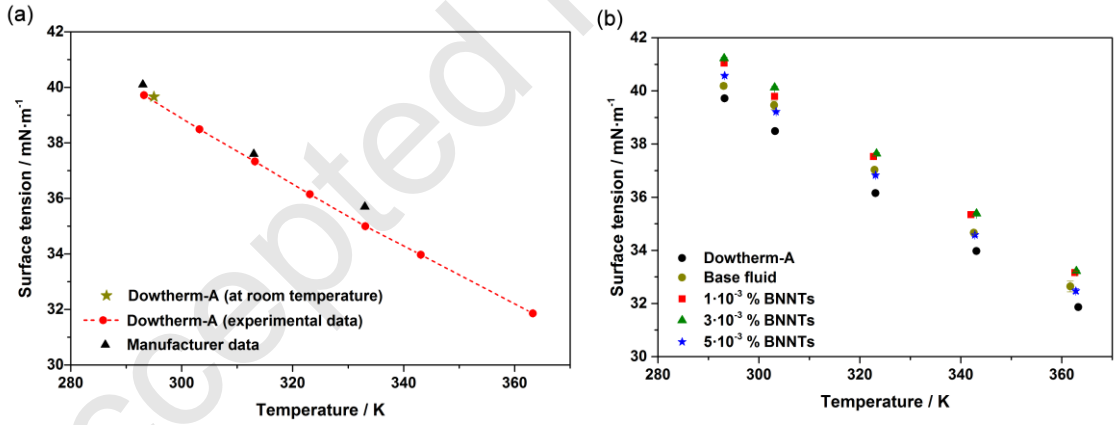

Figure 5. (a) Comparison of surface tension values obtained for Dowtherm A and those reported by the manufacturer. (b) Surface tension values obtained for the base fluid and for the nanofluids prepared, including the values of Dowtherm A for comparison purposes.

Table 1. Values of surface tension (γ), dynamic viscosity (μ), isobaric specific heat (C_P) and thermal conductivity (k) obtained for the fluid used (D-A, Dowtherm-A), for the base fluid (bf) and for nanofluids prepared.

T / K	γ / mN m^{-1}					μ / mPa s				
	D-A	bf	ϕ / vol.%			D-A	bf	ϕ / vol.%		
			3.4	5.8	8.6			3.4	5.8	8.6
283	--	--	--	--	--	6.036	6.185	6.298	6.387	6.461
293	39.72	40.19	41.05	41.23	40.58	4.211	4.444	4.507	4.532	4.581
303	38.49	39.46	39.79	40.13	39.22	3.161	3.381	3.394	3.456	3.541
323	36.15	37.03	37.53	37.64	36.83	1.966	2.089	2.172	2.178	2.201
343	33.97	34.66	35.34	35.38	34.58	1.344	1.455	1.475	1.507	1.543
363	31.86	32.64	33.16	33.22	32.47	0.981	1.095	1.120	1.153	1.159
T / K	C_P / J kg^{-1} K^{-1}					k / W m^{-1} K^{-1}				
	D-A	bf	ϕ / vol.%			D-A	bf	ϕ / vol.%		
			3.4	5.8	8.6			3.4	5.8	8.6
303	1567.1	1535.1	1571.5	1579.0	1588.8	0.147	0.146	0.152	0.149	0.157
323	1632.9	1603.3	1643.5	1640.4	1646.8	0.143	0.144	0.156	0.160	0.180
343	1703.4	1685.3	1703.9	1700.3	1696.1	0.142	0.149	0.173	0.182	0.186
363	1789.4	1765.9	1771.9	1759.6	1742.0	0.140	0.148	0.176	0.191	0.198

3.3. Density

Density is a property that significantly affects the heat transfer performance of nanofluids. Numerous studies reported increased efficiency of heat transfer fluids when density increases, typically due to an increase in particle loading [60]. Therefore, the density of the nanofluids was measured when they were considered stable. Density was measured by pycnometry. The volume fraction was calculated according to $\phi = (\rho_{nf} - \rho_{bf})/(\rho_{nt} - \rho_{bf})$, as is shown above. The base fluid is considered the eutectic mixture (Dowtherm A) with the surfactant Triton X-100, prepared under the same conditions and proportions as the nanofluids, as described in the experimental section. Table 2 shows that the density values of nanofluids obviously increase with volume fraction of nanofluid, an d decrease with temperature.

Table 2. Density values for the base fluid and the nanofluids, and the volume fraction calculated at 293K.

10^3 wt.% BNNTs	ρ / kg m^{-3}					ϕ / vol.%*
	293K	303K	323K	343K	363K	
0.0 (base fluid)	1073.0	1065.0	1048.0	1032.9	1016.8	0.0
1	1084.0	1076.0	1059.0	1043.9	1027.8	3.4
3	1092.0	1084.0	1067.0	1051.9	1035.8	5.8
5	1101.0	1092.9	1076.0	1060.9	1044.8	8.6

*volume fraction values calculated at 293K.

3.4. Rheological properties

To evaluate how the presence of nanomaterial could affect the rheological behaviour of nanofluids, rheological measurements were carried out. In this sense viscosity plays a critical role in heat transfer applications because an increase in values of this property has a counter-productive effect on efficiency [61], apart from generating engineering problems such as obstructions, abrasions and possible drops in pressure. Therefore, it is essential to control increases in viscosity. Thus, the dynamic viscosity of Dowtherm A was measured in a range of working temperatures and compared with the manufacturer's data. The results are shown in Figure 6a. Viscosity decreases while temperature increases, and the AAD% is around 1.9% at room temperature. Also, flow curves for Dowtherm A, the base fluid and each nanofluid at different temperatures are reported in Figure 6b to check the Newtonian behaviour within the investigated shear range rate. It was observed that the addition of surfactant caused a low increase in viscosity with regard to Dowtherm A. Moreover, the addition of BNNTs slightly affects the increase in viscosity values, as Figure 6c illustrates. Finally, Figure 6d shows the dynamic viscosity increase (DVI) for each nanofluid versus temperature. An increase of up to 6% in viscosity values is observed for the nanofluid with the highest concentration of BNNTs at 363K. The values of dynamic viscosity obtained are shown in Table 1.

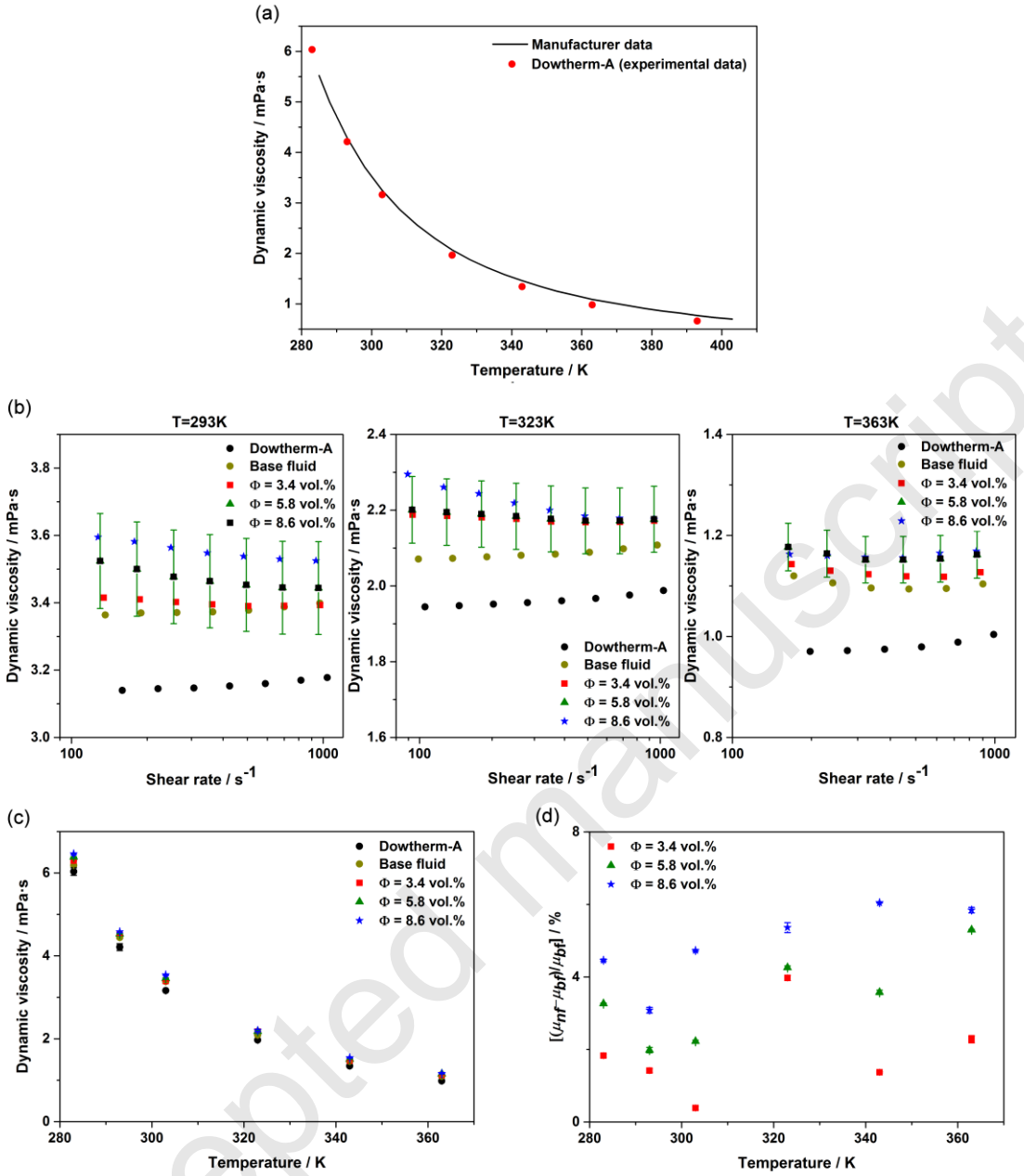

Figure 6. (a) Dynamic viscosity values measured for Dowtherm A compared with the values supplied by the manufacturer. (b) Dynamic viscosity values measured for the nanofluids prepared. The values for Dowtherm A and for the base fluid are included for comparison purposes. Representative error bars are included in one data set. (c) Evolution with temperature for the viscosity values measured. (d) Dynamic viscosity increase (DVI) for each nanofluid versus temperature.

3.5. Isobaric Specific Heat

Isobaric specific heat reveals the amount of heat that is required to change the temperature of a material and therefore plays an essential role in the heat transfer process. In fact, it contributes to determining the thermal conductivity through equation (2). To evaluate the method mentioned in section 2, the isobaric specific heat of Dowtherm A was measured and compared with the values provided by the supplier. At 298K, the experimental value obtained was 1537.7 J Kg^{-1} K^{-1} and the theoretical one is 1587 J Kg^{-1} K^{-1}, an uncertainty of around 3%. The isobaric specific heat of the base fluid and each nanofluid was measured in a range of temperatures between 303 and 363K. The values obtained versus temperature and volume fraction are shown in Figure 7, and some specific values are shown in Table 1. The values for the base fluid are lower than for the fluid with surfactant, so the presence of surfactant decreases the isobaric specific heat of the fluid. In turn, the addition of nanomaterial counters this effect, resulting in the nanofluids showing similar isobaric specific heat values to Dowtherm A and higher values than the base fluid. Since the isobaric specific heat of solids is generally lower than that of fluids, it is reasonable to expect that the suspension of solids could cause a decrease in isobaric specific heat values [39, 62, 63]. However, other authors have reported an increase in isobaric specific heat values when a nanomaterial is suspended within a fluid [14, 16, 64]. This is typically explained by an internal structure [65, 66], which is created by a interaction between the nanomaterial and base fluid. Furthermore, this internal structure can be affected by the nature of the components of the nanofluid, concentration of nanomaterial, agglomeration, number of interactions, etc.

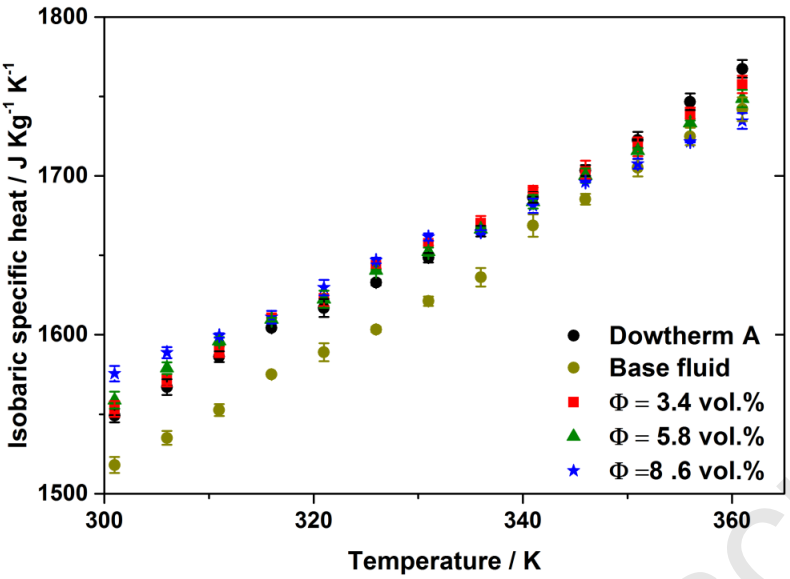

Figure 7. Isobaric specific heat values obtained for the fluid, the base fluid and the nanofluids versus temperature and volume fraction.

3.6. Thermal conductivity

Thermal conductivity was measured from 303K to 363K, the values obtained being shown in Figure 8a, and in Table 1. The evolution of the thermal conductivity with regard to temperature and volume fraction is observed. The thermal conductivity of Dowtherm A decreases with temperature, whereas the values for the base fluid remain practically constant. However, in the case of the nanofluids, the thermal conductivity increases with temperature and the concentration of nanomaterial. Thermal conductivity enhancement (TCE) with regard to the base fluid was calculated as $100 \cdot (k_{nf} - k_{bf})/k_{bf}$. Figure 8b shows the thermal conductivity enhancement for the nanofluids prepared with regard to the temperature and volume fraction. An increase in thermal conductivity was observed for all the nanofluids at all the measured temperatures. Indeed, the nanofluid with the highest volume fraction presented an increase of 33% at 363K.

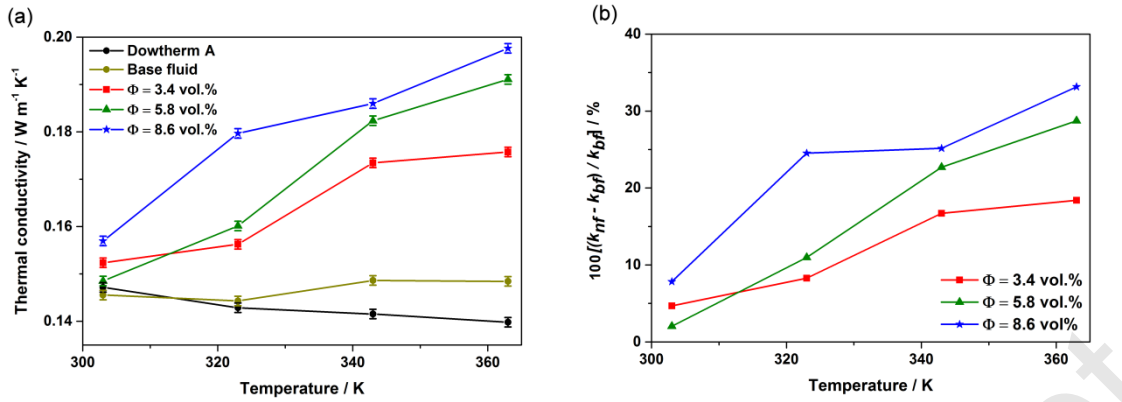

Figure 8. (a) Thermal conductivity values obtained for the fluid, the base fluid and the nanofluids with regard to temperature and volume fraction. (b) Thermal conductivity enhancement obtained for each nanofluid.

These results are in accordance with the literature, which reports an enhancement of thermal conductivity with increases in the volume fraction of nanoparticles. An increase in thermal conductivity is indicative of a more efficient heat transfer [16, 64, 67]. Furthermore, using boron nitride materials, Taha-Tijerina et al. [9] demonstrated that a nanofluid with 2D fillers of hexagonal BN in a mineral oil present high thermal conductivity; Zhi et al. [23] obtained an improvement of up to ~2.6 times in the thermal conductivity of water using nanofluids at a fraction of 6 vol.%; and Li et al. [32] obtained an improvement in thermal conductivity of around 30% using 5.5 vol.% of BN nanoparticles in ethylene glycol.

An analysis using several models to evaluate the thermal conductivity with regard to volume fraction may be of interest in order to understand the way in which the heat conduction into the nanofluids takes place. The models used in this work for fitting the experimental results have been described previously. We consider the Maxwell model (see equation (6)) as a general model and the model reported by Xue (see equation (8)) which is specific for nanotubes. Thus, Figure 7 shows the plot of the Maxwell model and

the Xue model and the experimental results for comparison purposes at several temperatures. Both models are able to predict the experimental results at 323K, and are close to the experimental values at 303 and 343K. However, at higher temperatures (363K) the experimental values are higher than the predicted values for both models suggesting that new conduction mechanisms may occur at higher temperatures. This is typically explained by the contribution of Brownian motion, and assuming that this mechanism can be considered separately, the total effective thermal conductivity can be considered as the sum of the terms related to static conductivity and Brownian motion; that is, $k_{nf} = k_{static} + k_{brownian}$. The contribution of the Brownian motion was considered from the model reported by Xuan et al (see equation (9)). Figure 9 shows the plot for these models. In all cases, an overestimated contribution of Brownian motion is predicted by the Xuan model. Thus, the increase in thermal conductivity at higher temperatures is not well predicted for Brownian motion. Further research will be needed to understand the behaviour of the thermal conductivity of these nanofluids at higher temperatures.

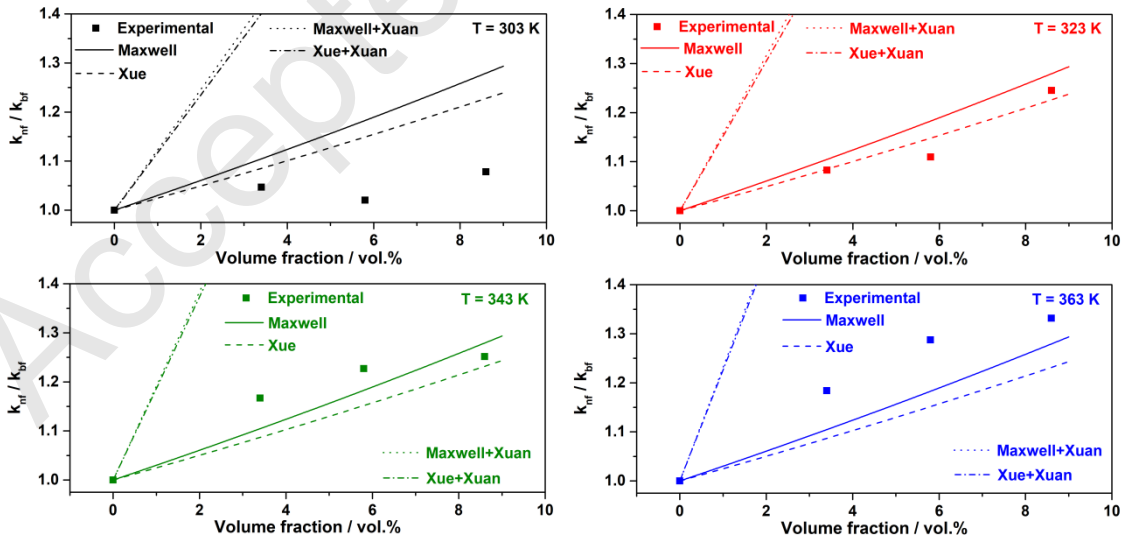

Figure 9. Thermal conductivity values for the nanofluids prepared and the representation of several theoretical models for thermal conductivity at 303, 323, 343 and 363K.

3.7. Performance of nanofluids

To verify the possible enhancement of the heat transfer process under turbulent flow conditions such as those found in CSP plants and the applicability of nanofluids in these plants, the Dittus-Boelter equation (see equation (2)) was used as a *Figure of Merit* (*FoM*). Figure 10a shows the values obtained for this *FoM* versus temperature and volume fraction. All the nanofluids present improvements in the heat transfer coefficient. An enhancement of up to 18% was obtained at 363 K for the nanofluids with the highest volume fraction of BNNTs. And higher values of the heat transfer coefficient lead to lower thermal losses, and therefore to an increase in the thermal efficiency of the collector [46, 47]. Moreover, friction factor *f* of base fluid and nanofluids evaluated from equation (3) for all concentrations and temperatures is reported in Figure 11. Such an evaluation was done considering an inner tube diameter (D = 0.066m) and flow rates (100-300 L/min) used in [46,47]. Obviously, an increase in flow rate leads to an increase of *Re*. For a fixed flow rate, a slight change in *Re* is observed due to the modification of viscosity and density with the presence of nanoparticles, as is shown above. Specifically, *Re* decreases with volume fraction increase as viscosity increase is more important that density enhancement. At same flow rate, a very slight increase of *f* with volume fraction is evidenced. Temperature increase leads to enhancement of *Re* and reduction in *f* due to evolution of density and viscosity with temperature. Finally, Figure 11 shows that thermal efficiency of collector with nanofluids will be not significantly penalized by friction factor increase that is beneficial in practical use.

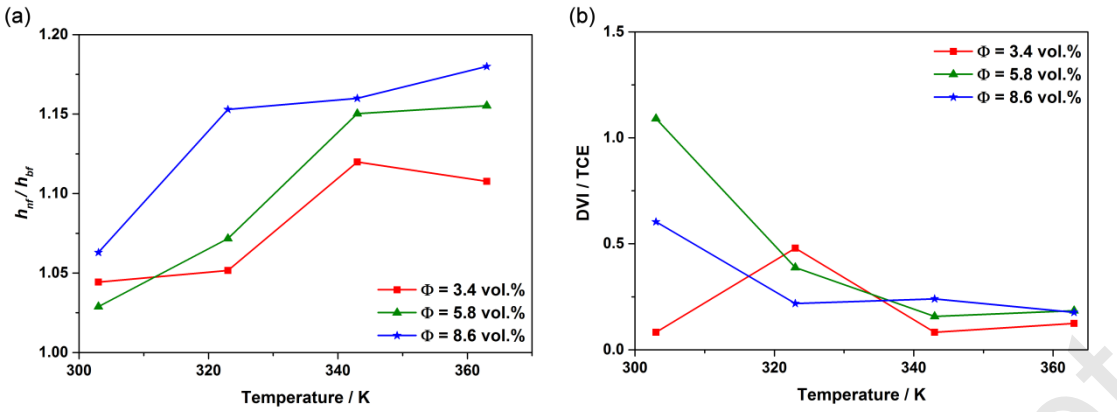

Figure 10. (a) Ratio of the heat transfer coefficient of nanofluids and base fluid versus temperature and volume fraction. (b) Ratio of the dynamic viscosity increase (DVI) and thermal conductivity enhancement (TCE) versus temperature and volume fraction.

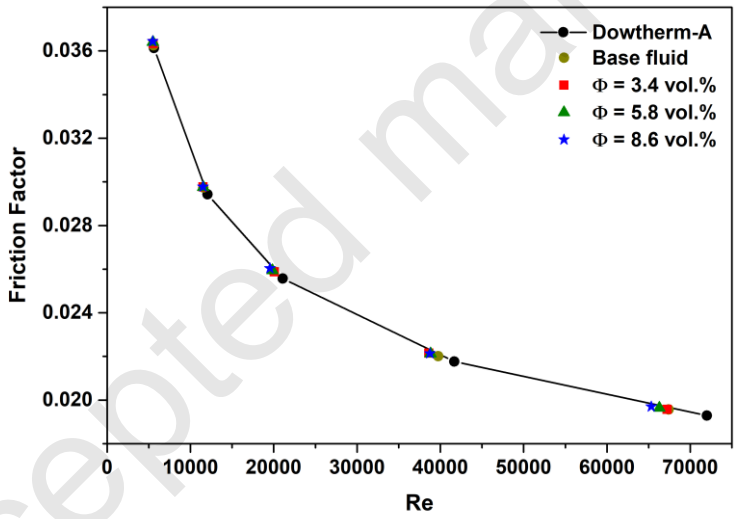

Figure 11. Friction factor of base fluid and nanofluids – influence of concentration, temperature and flow rate.

Also, under laminar flow conditions the criterion of Prasher (see equation (4)) was considered. Figure 10b shows the values obtained for this ratio, with all the nanofluids prepared being shown to fulfil the requirement described by Prasher for laminar flow conditions, all the nanofluids behaving similarly at higher temperatures.

It is also possible to compare the use of the nanofluids in CSP plants with that of the typical HTF used, namely Dowtherm A, by means of the analysis of the useful energy production defined in equation (5). From this equation, higher values of the heat transfer coefficient lead to lower values of the temperature in the receiver and consequently to lower thermal losses. This is the fact that increases the collector thermal efficiency. From equation (5), the decrease of the ΔT (that is $T_s - T_{fm}$) gives us the idea that the thermal efficiency of the collector is improved. Therefore, we can plot the ratio of ΔT between nanofluids and base fluid, to test the improvement in the thermal efficiency. Mathematically, from equation (5), this ratio is expressed as $\left[\left(T_s - T_{fm}\right)_{nf} / \left(T_s - T_{fm}\right)_{HTF}\right] = \left(h_{HTF}/h_{nf}\right)$. To evaluate this expression, the ratio of the heat transfer coefficient was determined from the Dittus-Boelter equation, the values of thermal conductivity, isobaric specific heat and dynamic viscosity were measured, and the values of the density of the HTF typically used in CSP plants were obtained from the supplier. Thus, Figure 12 shows the ratio between $\left[\left(T_s - T_{fm}\right)_{nf} / \left(T_s - T_{fm}\right)_{HTF}\right]$ versus the effective volume fraction for the nanofluids prepared. A value of this ratio lower than 1 means that the thermal losses decreases and the collector thermal efficiency is enhanced. Thus, the presence of BNNTs in the HTF leads to an increase in the outlet temperature in the system and therefore to an increase in the efficiency of the collectors.

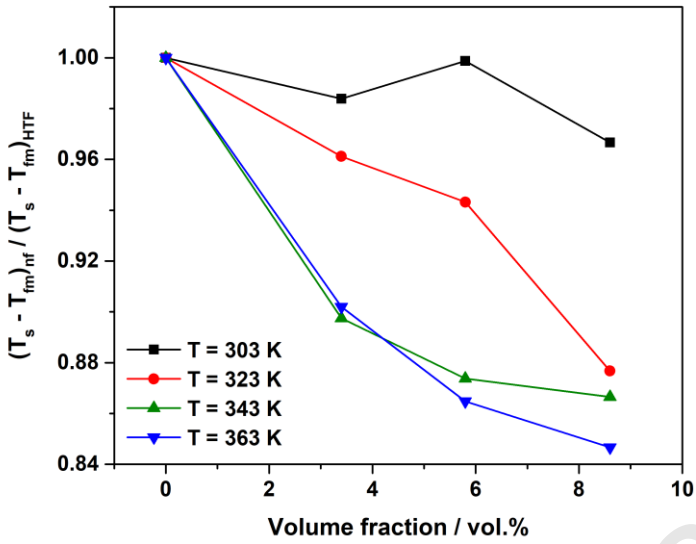

Figure 12. Analysis of the collector thermal efficiency using the nanofluids prepared.

In summary, according to the results obtained, the nanofluid with a mass concentration of 5·10-3 wt.% (ϕ = 8.6 vol.%) seems to be the most promising nanofluids in this work, showing an increase in thermal conductivity up to 33% at 363K. This value is interesting according to other values reported in the literature using the same base fluid, typically used in CSP plants. The increase in thermal conductivity obtained is similar to those reported in the literature using synthetic oils. For example, Wang et al. reported an increase in thermal conductivity about 36% for graphite/oil nanofluids, Yasinskiy et al. obtained an enhancement up to 25.8% for TiO_2 based nanofluids using the base fluid of this work, and also lower increases of 20% and 12.5% for Cu-based nanofluids or 6% for Ag-nanofluids have been reported. Therefore, the nanofluids reported in this work are of interest for solar thermal applications.

Finally, for its potential application in CSP plants, which work at high temperature, the nanofluid defined as the most promising, that with the highest volume fraction of BNNTs, was used in successive thermal cycles, reaching 573 K, following the procedure described

before. Figure 13a shows the results obtained of extinction coefficient at λ=335 registered from the UV-Vis spectra recorded before and after of each cycle. After first cycles, we can observe an increase in the extinction coefficient after the cycle, which may be because the heat applied provokes a large number of collisions in the heart of nanofluids that resulting in a more amount of nanomaterial in suspension, due to breakdown of some agglomerates. After five cycles, the changes in the extinction coefficient values are not significant, therefore the nanofluid system tends to some kind of stability. Moreover, the breakdown of agglomerates would lead agglomerates with lower sizes. Figure 13b shows the values of the particle size obtained before and after each thermal cycle. In some cases, two size distributions are obtained, as is described above (see Figure 3). In general, we can observe the agglomerate size decreases after heating, and also a tendency to reduce the agglomerate size after 10 cycles. But the decrease of size in the last cycles is lower, thus the nanofluid tends to stability, which is coherent with the extinction coefficient results. Moreover, the signal obtained by DLS shows more intense and narrow peaks after than before the cycle, as is shown in Figure 13c. Finally, Figure 13c shows STEM images from solid samples extracted before the first cycle and after the tenth cycle. In this image, isolated nanotubes have been observed. As we can observe, significant differences between the images taken before and after cycles have not been observed. And also, the diameter of the nanotubes isolated are very similar to that measured for BNNTs before preparing nanofluids (see Figure 1). Thus, no significant changes in the nano-morphology have occurred during the thermal cycles.

In summary, in terms of stability, heating processes did not produce substantial changes in the nanofluid. An increase in extinction coefficient and a decreasing in particle size towards stability were observed, probably because of the heat promotes nanomaterial

movements and collisions, generating more amount of nanomaterial in suspension with lower sizes.

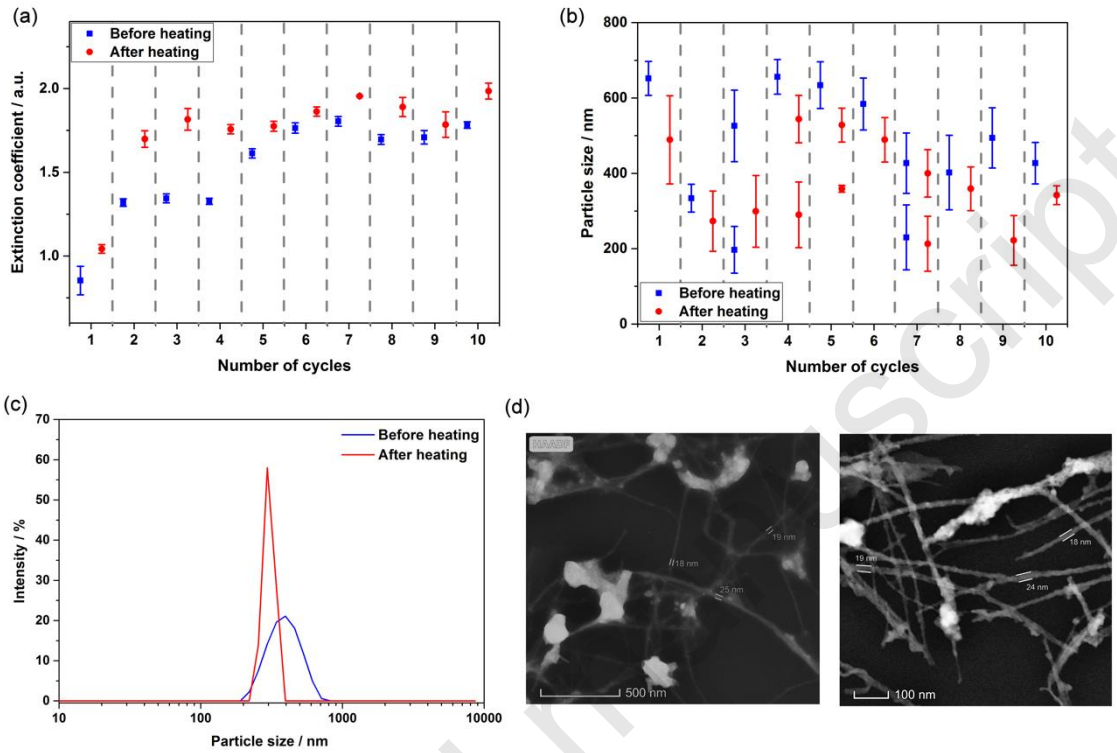

Figure 13. Extinction coefficient values obtained at λ = 335 nm (a), and particle size values (b) for the nanofluid with the highest concentration before and after thermal cycles. Example of the size distribution (c) and STEM images (d) before and after thermal cycles.

4. Conclusions

In summary, nanofluids based on boron nitride nanotubes dispersed in a heat transfer fluid commonly used in Concentrating Solar Power plants were prepared and characterized. Triton-X 100 was used as the surfactant. The nanofluids prepared were studied to determine their stability, surface tension, rheological and thermal properties.

All the nanofluids presented suitable stability. Measurements from ultraviolet-visible spectroscopy revealed stability after their preparation with a moderate decrease in

extinction of radiation. Particle size measurements showed two different distribution sizes with a similar intensity of about 200-300 nm and 400-600 nm. The ζ-potential values placed the nanofluids within the stable range. In addition, the presence of surfactant and BNNTs did not result in an observable change in surface tension values.

Regarding their rheological properties, the nanofluids presented higher viscosity values than the base fluid, around 6% for the nanofluids with the highest concentration of nanomaterial, with a Newtonian behaviour in all nanofluids within the shear range studied.

Concerning the thermal properties, the addition of surfactant led to a decrease in isobaric specific heat values and relatively constant thermal conductivity with regard to increases in temperature. However, the BNNT nanofluids showed a higher isobaric specific heat than the base fluid and an improvement in thermal conductivity with regard to the base fluid of up to 33% in the case of the nanofluid with highest nanomaterial concentration. Also, the efficiency of the nanofluids was estimated and an enhancement of 18% was obtained, and thermal efficiency of collector with nanofluids will be not significantly penalized by friction factor increase that is beneficial in practical use. Finally, good stability for the nanofluids was found at high temperature thanks to the analysis of the thermal cycles reaching 573 K.

Thus, the conclusion can be drawn that BNNT-based nanofluids present a promising future alternative to the heat transfer fluid commonly used in Concentrating Solar Power plants.

Acknowledgements

We thank to the Ministerio de Economía y Competitividad (MINECO) of the Spanish Government for funding Grant No. ENE2014-58085-R and for the financial support

related to measurements of thermal properties, which were carried out using devices acquired under Grant No. UNCA15-CE-2945.

Roberto Gómez-Villarejo acknowledges EU COST for the STSM Grant with reference COST-STSM-CA15119-37968 linked to the Cost Action “Overcoming Barriers to Nanofluids Market Uptake (NANOUPTAKE)”.

References

[1] S.U.S. Choi, J.A. Eastman, Enhancing thermal conductivity of fluids with nanoparticles, ASME-Publications-Fed 231 (1995) 99-106.
[2] T.P. Teng, Y.H. Hung, T.C. Teng, H.E. Mo, H.G. Hsu, The effect of alumina/water nanofluid particle size on thermal conductivity, Applied Thermal Engineering 30(14) (2010) 2213-2218.
[3] Y. Gao, H. Wang, A.P. Sasmito, A.S. Mujumdar, Measurement and modeling of thermal conductivity of graphene nanoplatelet water and ethylene glycol base nanofluids, International Journal of Heat and Mass Transfer 123 (2018) 97-109.
[4] X. Li, C. Zou, T. Wang, X. Lei, Rheological behavior of ethylene glycol-based SiC nanofluids, International Journal of Heat and Mass Transfer 84 (2015) 925-930.
[5] Y. Li, J. Fernández-Seara, K. Du, Á.Á. Pardiñas, L.L. Latas, W. Jiang, Experimental investigation on heat transfer and pressure drop of ZnO/ethylene glycol-water nanofluids in transition flow, Applied Thermal Engineering 93 (2016) 537-548.
[6] G. Żyła, J. Fal, Viscosity, thermal and electrical conductivity of silicon dioxide–ethylene glycol transparent nanofluids: An experimental studies, Thermochimica Acta 650 (2017) 106-113.
[7] M. Kole, T.K. Dey, Role of interfacial layer and clustering on the effective thermal conductivity of CuO–gear oil nanofluids, Experimental Thermal and Fluid Science 35(7) (2011) 1490-1495.
[8] B. Wang, X. Wang, W. Lou, J. Hao, Thermal conductivity and rheological properties of graphite/oil nanofluids, Colloids and Surfaces A: Physicochemical and Engineering Aspects 414 (2012) 125-131.
[9] J. Taha-Tijerina, T.N. Narayanan, G. Gao, M. Rohde, D.A. Tsentalovich, M. Pasquali, P.M. Ajayan, Electrically Insulating Thermal Nano-Oils Using 2D Fillers, ACS Nano 6(2) (2012) 1214-1220.
[10] U. Desideri, F. Zepparelli, V. Morettini, E. Garroni, Comparative analysis of concentrating solar power and photovoltaic technologies: Technical and environmental evaluations, Applied Energy 102 (2013) 765-784.
[11] V. Devabhaktuni, M. Alam, S. Depuru, R.C. Green, D. Nims, C. Near, Solar energy: Trends and enabling technologies, Renewable & Sustainable Energy Reviews 19 (2013) 555-564.
[12] J. Khan, M.H. Arsalan, Solar power technologies for sustainable electricity generation - A review, Renewable & Sustainable Energy Reviews 55 (2016) 414-425.
[13] G. Peiró, J. Gasia, L. Miró, C. Prieto, L.F. Cabeza, Influence of the heat transfer fluid in a CSP plant molten salts charging process, Renewable Energy 113 (2017) 148-158.
[14] D. Singh, E.V. Timofeeva, M.R. Moravek, S. Cingarapu, W. Yu, T. Fischer, S. Mathur, Use of metallic nanoparticles to improve the thermophysical properties of organic heat transfer fluids used in concentrated solar power, Solar Energy 105 (2014) 468-478.
[15] N. Nikkam, M. Ghanbarpour, M. Saleemi, E.B. Haghighi, R. Khodabandeh, M. Muhammed, B. Palm, M.S. Toprak, Experimental investigation on thermo-physical properties of copper/diethylene glycol nanofluids fabricated via microwave-assisted route, Applied Thermal Engineering 65(1) (2014) 158-165.
[16] J. Navas, A. Sánchez-Coronilla, E.I. Martín, M. Teruel, J.J. Gallardo, T. Aguilar, R. Gómez-Villarejo, R. Alcántara, C. Fernández-Lorenzo, J.C. Piñero, J. Martín-Calleja, On the enhancement of heat transfer fluid for concentrating solar power using Cu and Ni nanofluids: An experimental and molecular dynamics study, Nano Energy 27 (2016) 213-224.

[17] T. Aguilar, J. Navas, A. Sánchez-Coronilla, E.I. Martín, J.J. Gallardo, P. Martínez-Merino, R. Gómez-Villarejo, J.C. Piñero, R. Alcántara, C. Fernández-Lorenzo, Investigation of enhanced thermal properties in NiO-based nanofluids for concentrating solar power applications: A molecular dynamics and experimental analysis, Applied Energy 211 (2018) 677-688.
[18] A. Mwesigye, Z. Huan, J.P. Meyer, Thermodynamic optimisation of the performance of a parabolic trough receiver using synthetic oil–Al2O3 nanofluid, Applied Energy 156 (2015) 398-412.
[19] A. Yasinskiy, J. Navas, T. Aguilar, R. Alcántara, J.J. Gallardo, A. Sánchez-Coronilla, E.I. Martín, D. De Los Santos, C. Fernández-Lorenzo, Dramatically enhanced thermal properties for TiO2-based nanofluids for being used as heat transfer fluids in concentrating solar power plants, Renewable Energy 119 (2018) 809-819.
[20] Z. Hajjar, A.m. Rashidi, A. Ghozatloo, Enhanced thermal conductivities of graphene oxide nanofluids, International Communications in Heat and Mass Transfer 57 (2014) 128-131.
[21] M.K. Samani, N. Khosravian, G.C.K. Chen, M. Shakerzadeh, D. Baillargeat, B.K. Tay, Thermal conductivity of individual multiwalled carbon nanotubes, International Journal of Thermal Sciences 62 (2012) 40-43.
[22] A. Nasiri, M. Shariaty-Niasar, A.M. Rashidi, R. Khodafarin, Effect of CNT structures on thermal conductivity and stability of nanofluid, International Journal of Heat and Mass Transfer 55(5) (2012) 1529-1535.
[23] C. Zhi, Y. Xu, Y. Bando, D. Golberg, Highly Thermo-conductive Fluid with Boron Nitride Nanofillers, ACS Nano 5(8) (2011) 6571-6577.
[24] T. Ishii, T. Sato, Y. Sekikawa, M. Iwata, Growth of whiskers of hexagonal boron nitride, Journal of Crystal Growth 52 (1981) 285-289.
[25] N.G. Chopra, R.J. Luyken, K. Cherrey, V.H. Crespi, M.L. Cohen, S.G. Louie, A. Zettl, Boron Nitride Nanotubes, Science 269(5226) (1995) 966-967.
[26] D. Golberg, Y. Bando, M. Eremets, K. Takemura, K. Kurashima, H. Yusa, Nanotubes in boron nitride laser heated at high pressure, Applied Physics Letters 69(14) (1996) 2045-2047.
[27] O.R. Lourie, C.R. Jones, B.M. Bartlett, P.C. Gibbons, R.S. Ruoff, W.E. Buhro, CVD Growth of Boron Nitride Nanotubes, Chemistry of Materials 12(7) (2000) 1808-1810.
[28] G. Żyła, J. Fal, J. Traciak, M. Gizowska, K. Perkowski, Huge thermal conductivity enhancement in boron nitride – ethylene glycol nanofluids, Materials Chemistry and Physics 180 (2016) 250-255.
[29] R. Ma, Y. Bando, H. Zhu, T. Sato, C. Xu, D. Wu, Hydrogen Uptake in Boron Nitride Nanotubes at Room Temperature, Journal of the American Chemical Society 124(26) (2002) 7672-7673.
[30] X. Blase, A. Rubio, S.G. Louie, M.L. Cohen, Stability and Band Gap Constancy of Boron Nitride Nanotubes, EPL (Europhysics Letters) 28(5) (1994) 335.
[31] C. Tang, Y. Bando, C. Liu, S. Fan, J. Zhang, X. Ding, D. Golberg, Thermal Conductivity of Nanostructured Boron Nitride Materials, The Journal of Physical Chemistry B 110(21) (2006) 10354-10357.
[32] Y. Li, J.e. Zhou, Z. Luo, S. Tung, E. Schneider, J. Wu, X. Li, Investigation on two abnormal phenomena about thermal conductivity enhancement of BN/EG nanofluids, Nanoscale Research Letters 6(1) (2011) 443.
[33] J. Taha-Tijerina, L. Peña-Paras, T.N. Narayanan, L. Garza, C. Lapray, J. Gonzalez, E. Palacios, D. Molina, A. García, D. Maldonado, P.M. Ajayan, Multifunctional nanofluids with 2D nanosheets for thermal and tribological management, Wear 302(1) (2013) 1241-1248.

[34] B. İlhan, M. Kurt, H. Ertürk, Experimental investigation of heat transfer enhancement and viscosity change of hBN nanofluids, Experimental Thermal and Fluid Science 77 (2016) 272-283.
[35] M. Michael, A. Zagabathuni, S. Ghosh, S.K. Pabi, Thermo-physical properties of pure ethylene glycol and water–ethylene glycol mixture-based boron nitride nanofluids, Journal of Thermal Analysis and Calorimetry 1-12.
[36] R. Gómez-Villarejo, T. Aguilar, S. Hamze, P. Estellé, J. Navas, Experimental analysis of water-based nanofluids using boron nitride nanotubes with improved thermal properties, Journal of Molecular Liquids 277 (2019) 93-103.
[37] Y.J. Li, J.E. Zhou, S. Tung, E. Schneider, S.Q. Xi, A review on development of nanofluid preparation and characterization, Powder Technology 196(2) (2009) 89-101.
[38] X.F. Li, D.S. Zhu, X.J. Wang, N. Wang, J.W. Gao, H. Li, Thermal conductivity enhancement dependent pH and chemical surfactant for Cu-H2O nanofluids, Thermochimica Acta 469(1) (2008) 98-103.
[39] M. Chandrasekar, S. Suresh, T. Senthilkumar, Mechanisms proposed through experimental investigations on thermophysical properties and forced convective heat transfer characteristics of various nanofluids - A review, Renewable & Sustainable Energy Reviews 16(6) (2012) 3917-3938.
[40] D. Cabaleiro, P. Estellé, H. Navas, A. Desforges, B. Vigolo, Dynamic Viscosity and Surface Tension of Stable Graphene Oxide and Reduced Graphene Oxide Aqueous Nanofluids, Journal of Nanofluids 7(6) (2018) 1081-1088.
[41] S. Halelfadl, P. Estellé, B. Aladag, N. Doner, T. Maré, Viscosity of carbon nanotubes water based nanofluids: Influence of concentration and temperature, International Journal of Thermal Sciences, 71 (2013) 111-117.
[42] S.K. Das, N. Putra, P. Thiesen, W. Roetzel, Temperature dependence of thermal conductivity enhancement for nanofluids, Journal of Heat Transfer 125(4) (2003) 567-574.
[43] F.W. Dittus, L.M.K. Boelter, Pioneers in heat transfer - heat transfer in automobile radiators of the turbular type, University California Publications Eng. 2 (1930) 443-461.
[44] X. Fang, Y. Xu, Z. Zhou, New correlations of single-phase friction factor for turbulent pipe flow and evaluation of existing single-phase friction factor correlations, Nuclear Engineering and Design 241(3) (2011) 897-902.
[45] R. Prasher, D. Song, J. Wang, P. Phelan, Measurements of nanofluid viscosity and its implications for thermal applications, Applied Physics Letters 89(13) (2006) 133108.
[46] E. Bellos, C. Tzivanidis, Assessment of the thermal enhancement methods in parabolic trough collectors, International Journal of Energy and Environmental Engineering 9(1) (2018) 59-70.
[47] E. Bellos, C. Tzivanidis, Thermal efficiency enhancement of nanofluid-based parabolic trough collectors, Journal of Thermal Analysis and Calorimetry 135(1) (2019) 597-608.
[48] M.L. Levin, M.A. Miller, Maxwell's "Treatise on Electricity and Magnetism", Soviet Physics Uspekhi 24(11) (1981) 904.
[49] R.L. Hamilton, O.K. Crosser, Thermal conductivity of heterogeneous two-component systems, Industrial & Engineering Chemistry Fundamentals 1(3) (1962) 187-191.
[50] Q.Z. Xue, Model for thermal conductivity of carbon nanotube-based composites, Physica B: Condensed Matter 368(1) (2005) 302-307.
[51] Y.M. Xuan, Q. Li, W.F. Hu, Aggregation structure and thermal conductivity of nanofluids, Aiche Journal 49(4) (2003) 1038-1043.

[52] W. Yu, H.Q. Xie, A Review on Nanofluids: Preparation, Stability Mechanisms, and Applications, Journal of Nanomaterials (2012).
[53] S. Chakraborty, I. Sarkar, K. Haldar, S.K. Pal, S. Chakraborty, Synthesis of Cu-Al layered double hydroxide nanofluid and characterization of its thermal properties, Applied Clay Science 107 (2015) 98-108.
[54] W. Yu, H. Xie, L. Chen, Y. Li, Investigation on the thermal transport properties of ethylene glycol-based nanofluids containing copper nanoparticles, Powder Technology 197(3) (2010) 218-221.
[55] H. Chang, M.H. Tsai, Synthesis and characterization of ZnO nanoparticles having prism shape by a novel gas condensation process, Reviews on Advanced Materials Science 18 (2008) 734-743.
[56] Y.Y. Song, H. Bhadeshia, D.W. Suh, Stability of stainless-steel nanoparticle and water mixtures, Powder Technology 272 (2015) 34-44.
[57] G. Żyła, A. Witek, M. Gizowska, Rheological profile of boron nitride–ethylene glycol nanofluids, Journal of Applied Physics 117(1) (2015) 014302.
[58] S.K. Das, S.U.S. Choi, W. Yu, T. Pradeep, Nanofluids: science and technology John Wiley & Sons (2007).
[59] P. Estellé, D. Cabaleiro, G. Żyła, L. Lugo, S.M.S. Murshed, Current trends in surface tension and wetting behavior of nanofluids, Renewable and Sustainable Energy Reviews 94 (2018) 931-944.
[60] M.J. Pastoriza-Gallego, C. Casanova, R. Páramo, B. Barbés, J.L. Legido, M.M. Piñeiro, A study on stability and thermophysical properties (density and viscosity) of Al2O3 in water nanofluid, Journal of Applied Physics 106(6) (2009) 064301.
[61] S.M.S. Murshed, K.C. Leong, C. Yang, Investigations of thermal conductivity and viscosity of nanofluids, International Journal of Thermal Sciences, 47(5) (2008) 560-568.
[62] N.S.S. Mousavi, S. Kumar, Effective heat capacity of ferrofluids - Analytical approach, International Journal of Thermal Sciences 84 (2014) 267-274.
[63] D. Cabaleiro, C. Gracia-Fernández, J.L. Legido, L. Lugo, Specific heat of metal oxide nanofluids at high concentrations for heat transfer, International Journal of Heat and Mass Transfer 88 (2015) 872-879.
[64] R. Gómez-Villarejo, E.I. Martín, J. Navas, A. Sánchez-Coronilla, T. Aguilar, J.J. Gallardo, R. Alcántara, D. De los Santos, I. Carrillo-Berdugo, C. Fernández-Lorenzo, Ag-based nanofluidic system to enhance heat transfer fluids for concentrating solar power: Nano-level insights, Applied Energy 194 (2017) 19-29.
[65] D. Shin, D. Banerjee, Enhanced specific heat capacity of nanomaterials synthesized by dispersing silica nanoparticles in eutectic mixtures, Journal of Heat Transfer-Transactions of the ASME 135(3) (2013).
[66] D. Shin, D. Banerjee, Specific heat of nanofluids synthesized by dispersing alumina nanoparticles in alkali salt eutectic, International Journal of Heat and Mass Transfer 74 (2014) 210-214.
[67] E.V. Timofeeva, W. Yu, D.M. France, D. Singh, J.L. Routbort, Nanofluids for heat transfer: an engineering approach, Nanoscale Research Letters 6(1) (2011) 182.